J. Fluid Mech. (1982), *vol.* 123, *pp.* 143–153
Printed in Great Britain

Transition from regular to Mach reflection of shock waves Part 1. The effect of viscosity in the pseudosteady case

By H. G. HORNUNG† AND J. R. TAYLOR

Department of Physics, Faculty of Science, Australian National University, P.O. Box 4, Canberra, ACT 2600

(Received 10 July 1980 and in revised form 12 April 1982)

It is demonstrated experimentally that the influence of viscosity on the transition condition in pseudosteady flow is very significant. A mechanism is proposed for this effect, which explains the features of the observed behaviour. In particular, an experimental method of finding the inviscid transition condition, by extrapolation to infinite Reynolds number, gives excellent agreement with the calculated inviscid sonic criterion. It is thought that this provides the explanation for the usual persistence of regular reflection beyond the sonic condition.

1. Introduction

The condition for transition from regular to Mach reflection of shock waves has been observed to depend on whether it occurs in steady, pseudosteady‡ or unsteady flow (see e.g. Hornung, Oertel & Sandeman 1979; Henderson & Lozzi, 1975, 1979; Heilig 1969) and on whether the incident shock is 'strong' or 'weak' (see e.g. Henderson & Siegenthaler 1980). We consider the case of a strong shock in two-dimensional, pseudosteady flow of a thermally and calorically perfect, viscous gas.

In this regime the reflection configurations that occur can be classified into three types as shown in figure 1 (see e.g. Ben Dor & Glass 1979). For present purposes we collect all those configurations that exhibit a characteristic length in the vicinity of the reflection point (shown by figures 1*b*, *c*) into a single category and call it Mach reflection, since our main interest is in the condition for failure of regular reflection. The regular-reflection configuration (figure 1*a*) is expected to occur when the speed of the point P is greater than a_3, the speed of sound in region 3. Since no information about the leading edge of the wedge can then reach P, the flow near P cannot be influenced by it, and consequently, in the inviscid case, exhibits no lengthscale. The condition when P travels just at the speed a_3 is called the sonic condition. Let the shock angle at this condition be $\alpha = \alpha_s$.

A Galilean transformation of a regular reflection to a frame of reference moving with the point P makes the flow in the vicinity of P steady. In this frame, the wedge and the gas in region 1 move at a speed

$$V_1 = V_s/\sin\alpha. \tag{1}$$

The incident shock I deflects the flow towards the wall through an angle θ_I, and the reflected shock R deflects it back to a direction parallel to the wall (see figure 2*a*) through an angle

$$\theta_R = \theta_I. \tag{2}$$

† Present address: DFVLR-AVA, 34 Göttingen, Bunsenstr. 10, W. Germany.

‡ Linear growth of features with time.

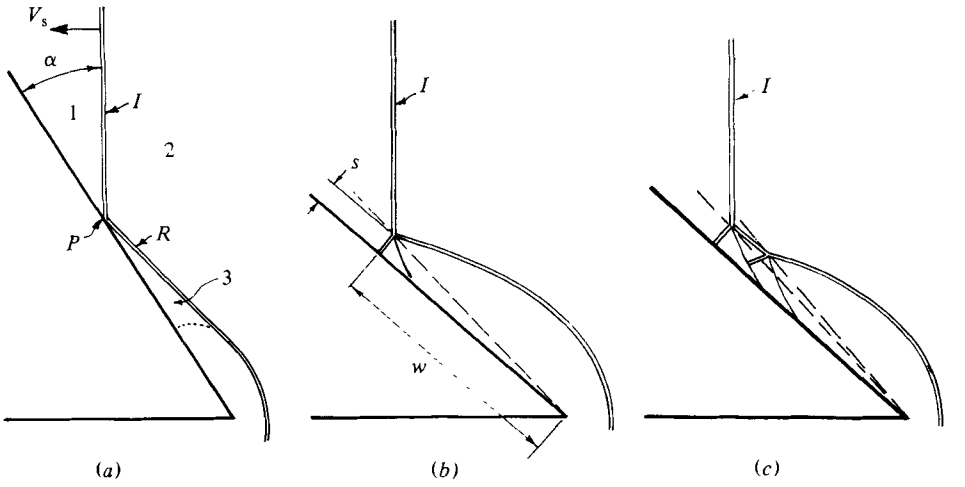

FIGURE 1. Pseudosteady-reflection configurations. The incident shock I travels into stationary gas at constant speed V_s from right to left and strikes the stationary wedge. P, reflection point; R, reflected shock. (*a*) Regular reflection: (*b*) Simple Mach reflection; · · · · · ·, range of corner signal. (*c*) Double Mach reflection. ═══, shock; ——, contact discontinuity; – –, triple-point trajectory.

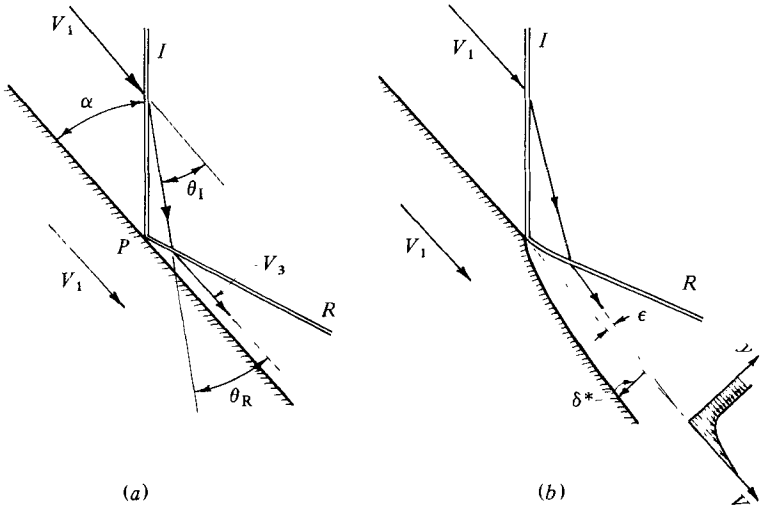

FIGURE 2. Regular reflection viewed from a reference frame moving with P. (*a*) Inviscid flow. (*b*) Inviscid model with boundary-layer displacement thickness δ^*.

As α is increased, θ_I increases until the reflected shock reaches the maximum deflection condition. Let $\alpha = \alpha_d$ at this point. The difference between α_d and α_s is approximately 0·1° and will be neglected in the following.

At this point we digress to define a 'strong' shock: the incident shock is called strong if the pressure in region 3, at the condition $\alpha = \alpha_d$, is greater than that after a shock travelling at speed V_1 into stationary gas at the conditions of region 1. This corresponds to an incident shock Mach number greater than the value at which $\alpha_d = \alpha_N$ (see figure 3, Hornung & Robinson 1982). For weak shocks, Henderson & Siegenthaler (1980) showed that the attenuation of the reflected shock is important.

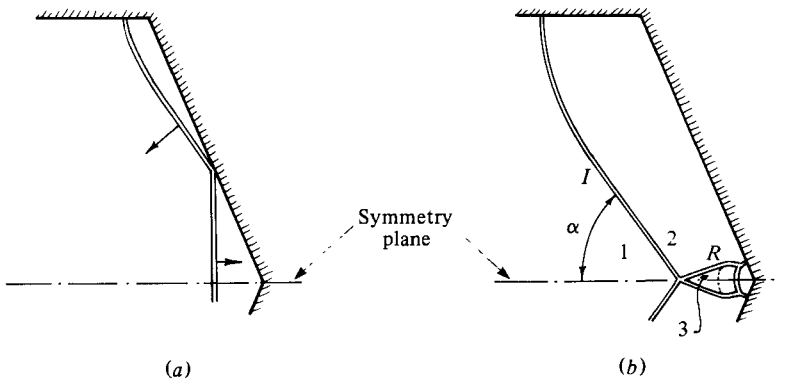

FIGURE 3. The symmetrical arrangement for pseudosteady flow avoids the boundary-layer problem. (*a*) Early time: the shock reflected from the oblique end wall of the shock tube becomes the 'incident' shock *I*. (*b*) Later: the features of the regular reflexion of *I* off the symmetry plane can be identified with those of figure 2(*a*).

Though regular reflection is not theoretically possible for $\alpha > \alpha_d$ in pseudosteady flow, experimental results indicate that the transition occurs at significantly positive values of $\alpha - \alpha_d$ (e.g. Bleakney & Taub 1949; Kawamura & Saito 1956; Henderson & Lozzi 1975). However, by using the symmetrical configuration shown in figure 3, which replaces the wedge surface by a plane of symmetry, both Smith (1959) and Henderson & Lozzi (1975, figures 5*a*, *b*) obtained results that give the transition angle α^* as α_d to within the experimental error, in agreement with theory. This difference, and the behaviour of the results of Takayama & Sekiguchi (1977) persuaded Hornung *et al.* (1979) to suggest a possible mechanism for the persistence of regular reflection beyond α_d, involving the viscous boundary layer on the wedge surface.

It is clear from figure 2 that $V_1 > V_3$, so that the boundary layer forming downstream of *P* on the wedge surface in region 3 has a velocity profile as sketched in figure 2(*b*), with a negative displacement thickness of magnitude $\delta^*(x)$. The flow direction can therefore have a significant component perpendicular to the wall in region 3. This would change (2) to

$$\theta_I - \theta_R = \epsilon > 0, \tag{3}$$

and therefore cause the maximum-deflection condition on the reflected shock to be shifted to a larger value of α. Hornung *et al.* (1979) tested this mechanism only by making crude estimates on their own results. We wish to emphasize that this mechanism is not related to the viscous growth of the shear layer at the contact discontinuity that occurs in a Mach reflection after the triple point (see e.g. Sternberg 1959; Skews 1971). The latter effect is not expected to influence the failure of regular reflection, because it is not present until a Mach reflection is established.

The experiment described in the following sections was designed specifically to test the hypothesis of Hornung *et al.* (1979) about the effect of viscosity by measuring the transition angle at different Reynolds numbers, but at constant shock Mach number, in order to find if there is any detectable dependence of α^* on Reynolds number, and, if so, to see if this dependence is consistent with simple boundary-layer ideas and with the inviscid value of α^*. Some of the results of this work have been reported by Taylor & Hornung (1980).

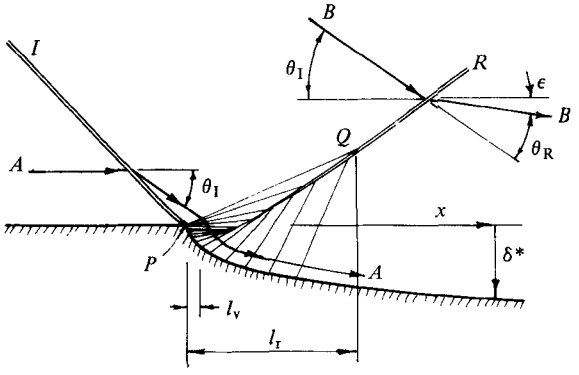

FIGURE 4. The inviscid model of the viscous effect defines the lengthscale l_r of the viscous regular reflexion.

2. Expected behaviour of α^* with Reynolds number

2.1. *The scale of the regular reflection*

Viewed in a frame of reference moving with the point P, the flow in the vicinity of the regular reflection point is steady. The presence of the boundary layer may be modelled by an inviscid flow with a displaced wall (see figure 4). (For a treatment of the problem of a shock-generated boundary layer, see Becker (1961).) In this model, a streamline A, passing through the incident shock I at a point close to the wall, is first deflected towards the wall by I. It then undergoes an isentropic expansion followed by an isentropic compression to make it follow the displaced wall. The compression steepens into a shock further downstream, however, so that a streamline passing through the incident shock at a point far from the wall is deflected back to a direction approximately parallel to the displaced wall by this reflected shock R. The scale of the features of this flow can conveniently be defined by the distance l_r between P and the point Q, the intersection of the leading characteristic from P with the reflected shock. Clearly, l_r will be scaled by the viscous lengthscale

$$l_v = \mu_3/\rho_3 V_3, \tag{4}$$

where μ is the viscosity, ρ the density and V the speed of the gas, and the subscript 3 refers to conditions in region 3. If $l_v = 0$ (inviscid flow) then $l_r = 0$, and the regular-reflection configuration is devoid of a lengthscale.

The shape of the displaced wall is given by

$$\frac{\delta^*}{x} = C_1\left(\frac{l_v}{x}\right)^{\frac{1}{2}} = C_1(Re_x)^{-\frac{1}{2}}, \tag{5}$$

where C_1 is a constant of order 1. It is assumed that $l_r \ll w$, where w is the distance from the leading edge of the wedge to P. Fairly straightforward estimates of the inviscid gasdynamics of the reflection (figure 4) show that

$$l_r/l_v \approx 10 \tag{6}$$

for the conditions of the experiment described in §3.

In order to estimate the effect of viscosity on the measured transition angle α^*, it is necessary to relate $\theta_I - \theta_R = \epsilon$ to l_v. However ϵ continues to decrease with distance downstream, and it is difficult to decide at which x it should be evaluated to determine the transition condition.

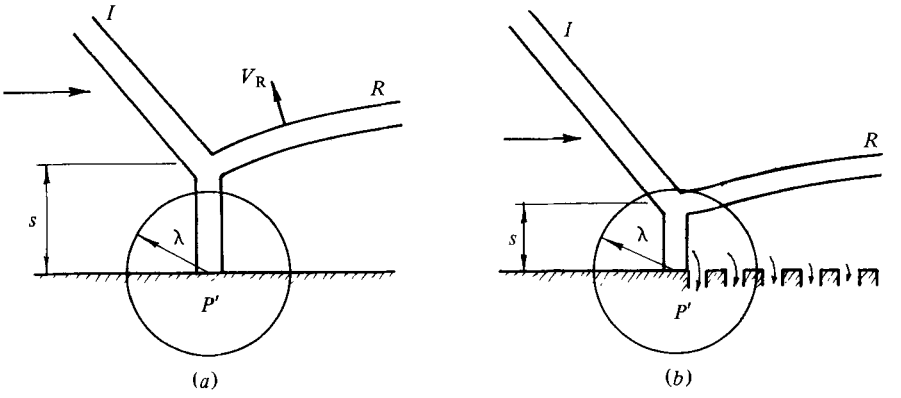

FIGURE 5. Illustrating how the viscous displacement effect can cause the Mach stem length s to become smaller than the smallest resolvable length λ, thus changing a Mach reflection to a regular reflection. (*a*) Inviscid flow. (*b*) Viscous effect modelled by distributed sinks along the wall.

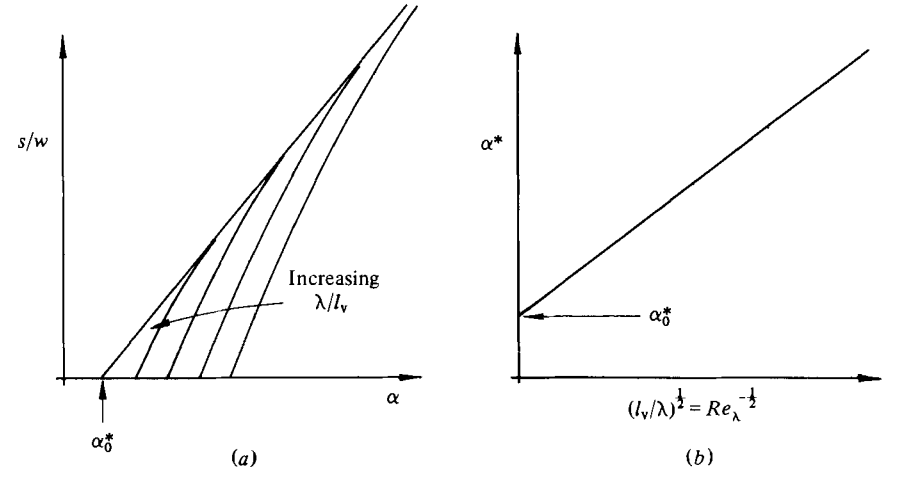

FIGURE 6. (*a*) Expected behaviour of the dimensionless Mach stem length with α. (*b*) Expected behaviour of the transition angle α^* with Reynolds number. The estimated slope of this line is 1·3 (see (11), (12)).

2.2. *The appropriate lengthscale for the Reynolds number*

For the purpose of determining this length, it is more convenient to consider the Mach-reflection configuration. Viewed from the frame of reference fixed in the point of intersection P' of the Mach stem and the wall, the flow is only steady in the immediate vicinity of the wall, since s grows with time (see figure 5). The rate of growth of s is determined by the reflected shock velocity V_R. The displacement effect of the boundary layer is equivalent to a removal of mass at the wall and can be modelled by a distributed sink along the wall.† This leads to a reduction of pressure and consequently to a reduction of V_R, and therefore of s. It may also be expected to shift the appearance of a Mach stem to higher α.

This last effect is illustrated by figures 5(*a*,*b*). The experimentally observed reflection configuration will be interpreted as a regular reflection if

$$s \leqslant \lambda, \tag{7}$$

† The displaced-wall model of §2.1 and this distributed sink model are equivalent.

V_s (km s^{-1}) $1{\cdot}75 \pm 0{\cdot}05$	M_s $5{\cdot}5 \pm 0{\cdot}2$	w (cm) 2–5		
p_1 (Torr)	5·0	10·0	25	70
l_v (μm) ($\alpha = 35°$)	1·58	0·79	0·32	0·112

TABLE 1. Experimental conditions

where λ is the smallest resolvable lengthscale of the observer. A circle of radius λ is drawn schematically about P' in figures 5(a, b). Since s will only be observed if it is greater than λ, the transition condition is characterized by the lengthscale λ. Therefore the range at which the strength of the displacement effect has to be evaluated for the purposes of the transition condition is λ.

When $s \approx \lambda$ only those distributed sinks that are within a distance of order λ can significantly affect V_R near the triple point. At a range of λ, the viscous displacement effect, as measured by $\epsilon = \theta_I - (\theta_R)_{x=\lambda}$ is given by

$$\epsilon = \left(\frac{d\delta^*}{dx}\right)_{x=\lambda} = \tfrac{1}{2}C_1\left(\frac{l_v}{\lambda}\right)^{\frac{1}{2}}. \tag{8}$$

By using the results of Mirels' (1956) calculations† and applying them to the boundary layer after a regular reflection at the conditions of our experiments (see table 1), the constant may be obtained as

$$C_1 = 3{\cdot}7. \tag{9}$$

Small changes of ϵ affect α^* in a linear fashion. Thus, a series of numerical computations of the inviscid regular reflection, made at the point where the reflected shock is at the maximum-deflection condition, for various values of ϵ, indicates that the linear approximation

$$\alpha^* = (\alpha^*)_{\epsilon=0} + C_2\epsilon, \tag{10}$$

with $C_2 = 0{\cdot}70$, applies to an accuracy better than $\pm 0{\cdot}2°$ in the range $35° < \alpha < 43°$ (for conditions as in table 1). Hence, for large $\lambda/l_v = Re_\lambda$, it may be expected that

$$\alpha^* = \alpha_0^* + C\left(\frac{l_v}{\lambda}\right)^{\frac{1}{2}} = \alpha_0^* + C(Re_\lambda)^{-\frac{1}{2}}, \tag{11}$$

where α_0^* is the inviscid transition angle at $l_v = 0$, and

$$C = \tfrac{1}{2}C_1C_2 = 1{\cdot}3. \tag{12}$$

2.3. *Behaviour at large Mach stem length*

When s becomes large compared with l_v, the effect of the displacement thickness on the speed of the reflected shock must decrease. This may be seen by comparing m_δ, the mass-flow rate in the boundary layer, with m_s, the total mass flow rate through the Mach stem. As $s/l_v \to \infty$, m_δ/m_s must clearly go to zero. Consequently, it may be expected that the effect of viscosity disappears as s/l_v increases. Putting this together with the usual behaviour of s/w with α (see e.g. Sandeman, Leitch & Hornung 1979) and with (11), it may be expected that the overall behaviour is as sketched in figures 6(a, b).

† See also Schlichting (1965).

3. Experiment

The experiment was conducted in the 7·6 cm diameter free-piston shock tube at ANU known as T3. The free-piston driver technique is particularly suitable here. This is because our experiment requires the same shock speed to be attained over a range of initial shock-tube pressure p_1. The free-piston technique supplies this with continuous variability, because the driver temperature can be chosen by adjusting the compression ratio of the adiabatic piston compression. One problem, however, is that the facility cannot easily be operated at low shock Mach number $M_s = V_s/a_1$.

To keep things as simple as possible, real-gas effects were avoided by choosing argon as test gas. Since this is relatively free of low-energy gas imperfections, a fairly high M_s can be used without violating the perfect-gas assumptions. By numerical computation of real-gas argon shock reflections, a suitable limit was found at $M_s = 5{\cdot}5$. Up to this value, and in the range of p_1 of our experiments, real-gas effects cause the inviscid transition angle α_d to change by less than 0·2°. The experimental conditions are presented in table 1 for clarity.

The shock was reflected for an adjustable wedge of 4 cm width, placed just outside the exit plane of the shock tube, which is enclosed in a large dump tank. The flow was made visible by the shadowgraph technique or by differential interferometry. The light source was a dye laser pumped by a nitrogen laser (see Sandeman *et al.* 1979). This was triggered from the last of four shock-timing stations with a preset delay to 'catch' the shock at the right point. The light source provided a flash of 5 ns duration at a wavelength of 589 ± 5 nm. Examples of the resolution that is typical of the photographs taken are given in figures 7 and 8. As can be seen, the resolution limit, measured e.g. by the shock thickness, is somewhere in the range

$$0{\cdot}1 \text{ mm} < \lambda < 0{\cdot}5 \text{ mm}. \tag{13}$$

4. Results and discussion

Measured values of the dimensionless Mach stem length s/w are plotted against the shock angle α in figure 9 for four values of p_1. As can be seen, the main behaviour is consistent with that of figure 6(*a*), though the results are not able to confirm the merging towards the inviscid limit at high s/w. The transition angle is obtained by extrapolating to zero s/w the straight lines fitted to the experimental points of figure 9. This value of α^* is plotted against $(l_v/\lambda)^{\frac{1}{2}}$ in figure 10, in which λ is chosen to match the slope to that estimated from theoretical arguments in §2.2 (equation 12). This match yields the smallest resolvable length in our experiments as

$$\lambda = 0{\cdot}22 \text{ mm}, \tag{14}$$

consistent with the range (13) estimated from the photographs.

Extrapolating the straight line in figure 10 to the inviscid limit produces an experimental value of the inviscid transition angle

$$(\alpha^*)_{l_v=0} = 35{\cdot}4 \pm 0{\cdot}5°. \tag{15}$$

This is in excellent agreement with the calculated inviscid detachment (or sonic) criterion

$$\alpha_d = 35{\cdot}4° \tag{16}$$

at $M_s = 5{\cdot}5$, $\gamma = \frac{5}{3}$. Note that this agreement is independent of the choice of λ. Thus the experimental behaviour confirms the proposed mechanism in every way.

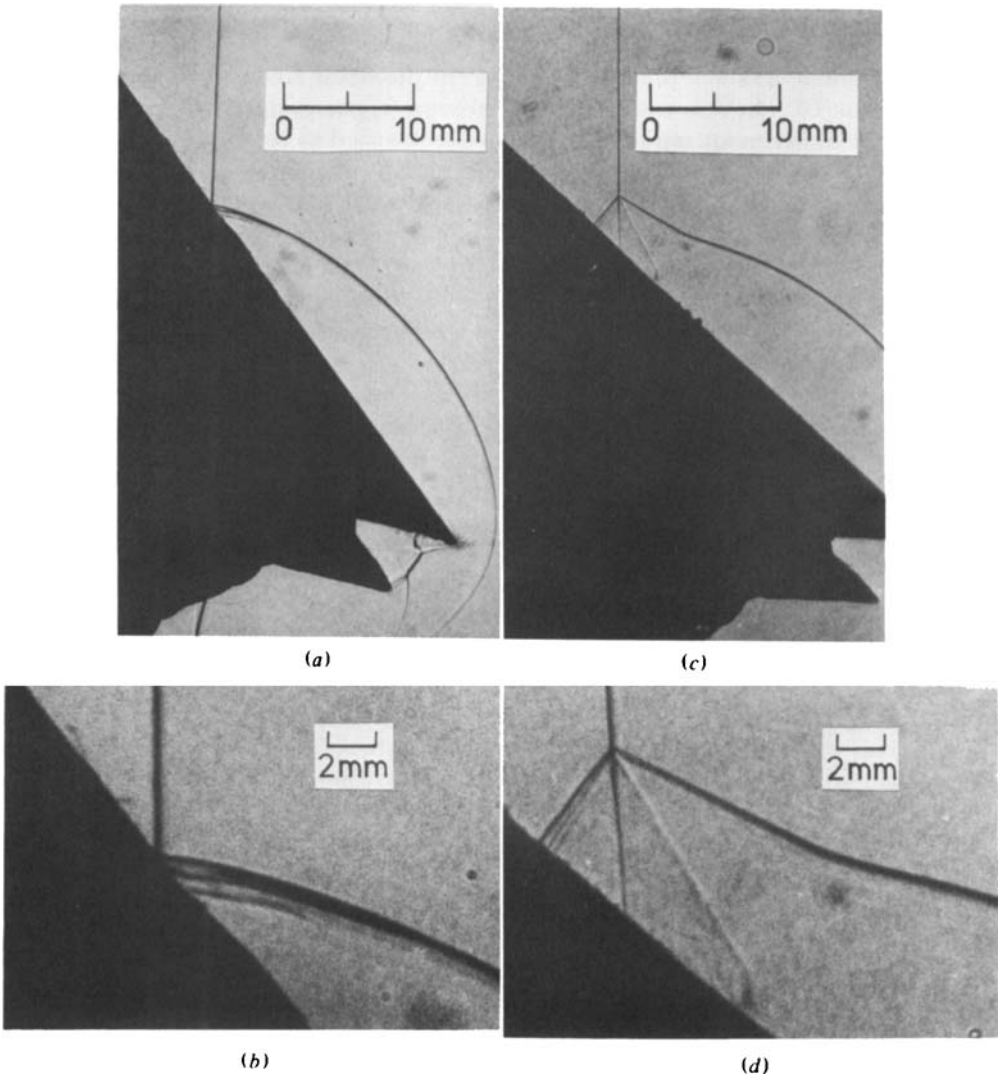

FIGURE 7. (*a*) Shadowgraph of reflection near transition. (*b*) Enlarged portion of (*a*). (*c*) Mach reflection. Note that the portion of the incident shock on the sides of the wedge is visible through the Mach reflection because the transverse width of the wedge is smaller than the shock-tube diameter. (*d*) Enlarged portion of (*c*).

Finally, it is necessary to discuss an alternative way of determining α_0^*. In our experiment the variation of the Reynolds number was achieved by varying l_v at constant λ. According to the mechanism we propose, one could equally effectively vary λ at constant l_v. To examine what would happen in that case, consider a particular one of the set of curves in figure 6(*a*). α^* is obtained by extrapolating this curve to zero s/w. If the error bar of the experimental measurements from which the curve is derived is increased, the curve effectively becomes thicker. Consequently the part of the curve that is used to extrapolate to zero s/w has to be further from $s/w = 0$. Hence the value of α^* obtained by the extrapolation decreases as λ increases. In other words: with a coarser resolution the observer needs to use a larger Mach stem length to be able to extrapolate to zero. With a large Mach stem length at constant l_v the importance of the displacement thickness is reduced. Unfortunately our experiments

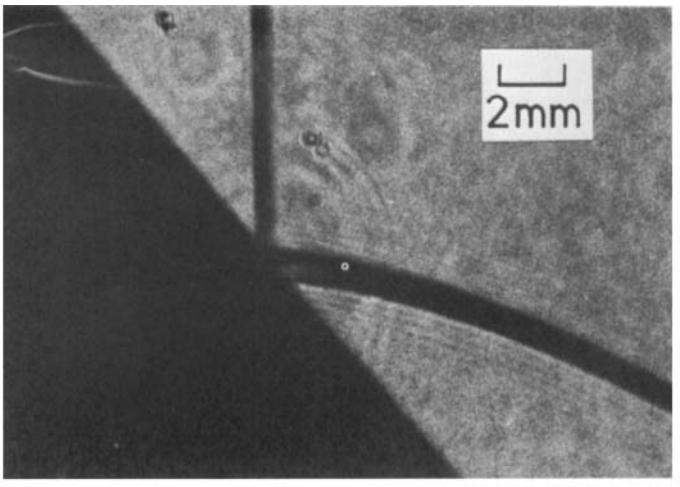

(*a*)

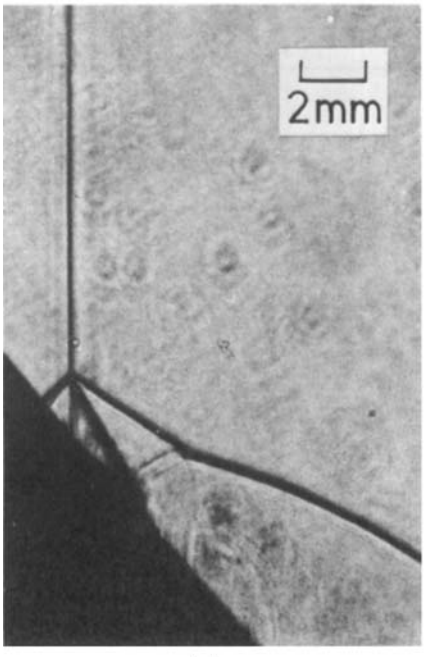

(*b*)

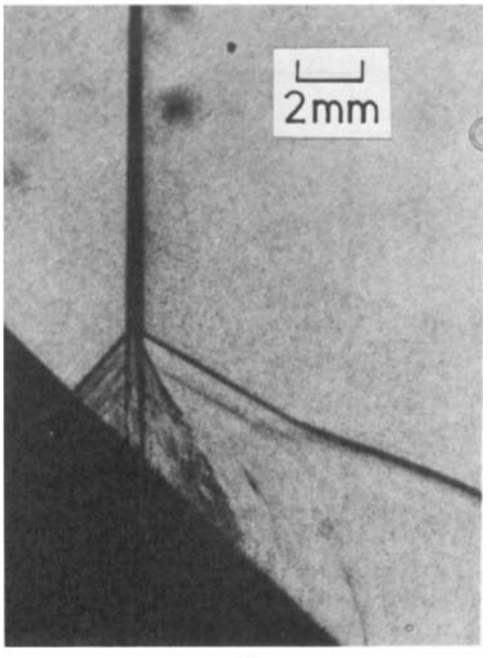

(*c*)

FIGURE 8. Shadowgraphs of detail around the reflection point for (*a*) regular, and (*b*, *c*) Mach reflection. Note the instability in the contact discontinuity in (*c*). The double image of the side portions of the incident shock in (*c*) indicates misalignment of the optics relative to the shock.

yield inaccurate results if the Mach stem length is allowed to become too large, because of the limited size of the shock tube. It was therefore better to vary l_v at the smallest achievable λ than to try to measure one of the curves of figure 6(*a*) up to the inviscid asymptote.

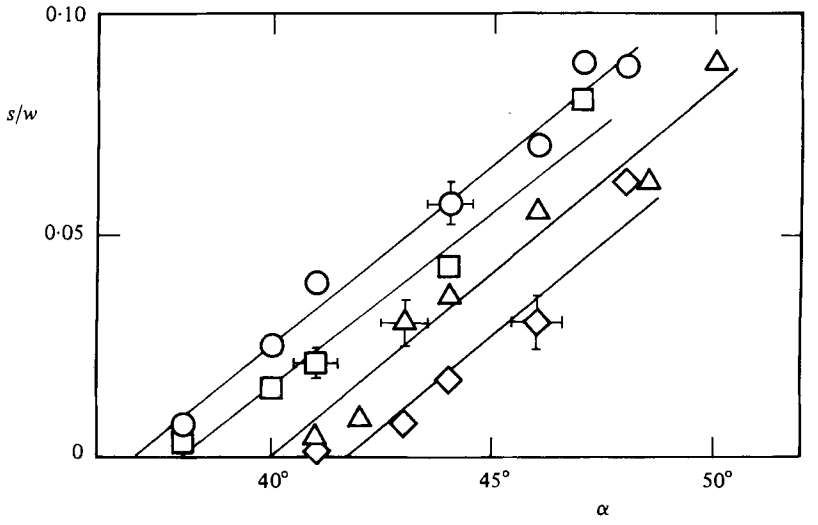

FIGURE 9. Experimental results. Dimensionless Mach stem length for: ○, $p_1 = 70$ Torr; □, 25 Torr; △, 10 Torr; ◇, 5·0 Torr.

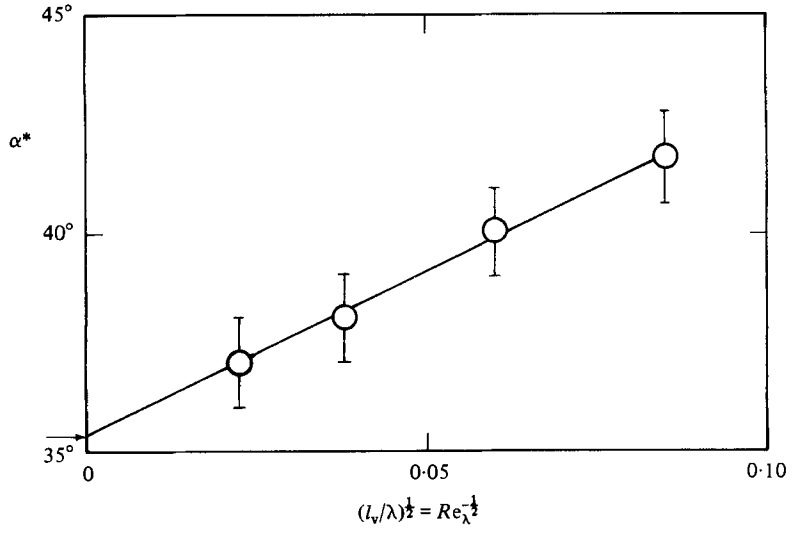

FIGURE 10. Experimental results: transition angle as a function of Reynolds number. Note the calculated inviscid value of α^* indicated by an arrow. Choosing $\lambda = 0{\cdot}22$ mm gives agreement of slope with theoretical estimate (11), (12).

5. Conclusions

The experiment shows that the transition to Mach reflection of strong shock waves in pseudosteady flow is significantly influenced by viscosity. In our experiments the effect reaches up to 7° in the shock angle. A mechanism is proposed which explains this increase of the transition shock angle quantitatively. We believe that this mechanism provides the explanation for the much-discussed persistence of regular reflection beyond the sonic criterion in pseudosteady flow.

This work was supported by the Australian Research Grants Committee.

REFERENCES

BECKER, E. 1961 *Prog. Aero. Sci.* **1**, 104–173.

BEN DOR, G. & GLASS, I. I. 1979 *J. Fluid Mech.* **92**, 459–596.

BLEAKNEY, W. & TAUB, A. H. 1949 *Rev. Mod. Phys.* **21**, 584–605.

HEILIG, W. 1969 *Dissertation*, University of Karlsruhe.

HENDERSON, L. F. & LOZZI, A. 1975 *J. Fluid Mech.* **68**, 139–155.

HENDERSON, L. F. & LOZZI, A. 1979 *J. Fluid Mech.* **94**, 541–559.

HENDERSON, L. F. & SIEGENTHALER, A. 1980 *Proc. R. Soc. Lond.* A **369**, 537–555.

HORNUNG, H. G., OERTEL, H. & SANDEMAN, R. J. 1979 *J. Fluid Mech.* **90**, 541–560.

HORNUNG, H. G. & ROBINSON, M. L. 1982 *J. Fluid Mech.* **123**, 155–164.

KAWAMURA, R. & SAITO, H. 1956 *J. Phys. Soc. Japan* **11**, 584–592.

MIRELS, H. 1956 *NACA Tech. Note* no. 3712.

SANDEMAN, R. J., LEITCH, A. M. & HORNUNG, H. G. 1979 In *Proc. 12th Int. Symp. on Shock Tubes and Waves, Jerusalem.*

SCHLICHTING, H. 1965 *Grenzschichttheorie*, §xv. f.1. Braun.

SKEWS, B. W. 1971 *C.A.S.I. Trans.* **4**, 99–107.

SMITH, W. R. 1959 *Phys. Fluids* **2**, 533–541.

STERNBERG, J. 1959 *Phys. Fluids* **2**, 179–206.

TAKAYAMA, K. & SEKIGUCHI, H. 1977 *Rep. Inst. High Speed Mech. Tohoku Univ.* **336**, 53–74.

TAYLOR, J. R. & HORNUNG, H. G. 1980 In *Proc. 7th Austral. Fluid Mech. Conf., Brisbane.*